## Experimental section

*Materials, electrode and cell preparation*

$LiCoO_2$ (LCO, Novarials) and $LiNi_{1/3}Co_{1/3}Mn_{1/3}O_2$ (NCM, MTI Corp.) powders were used for the electrode preparation with carbon black (Super P, Imerys) as conductive additive and polyvinylidene fluoride (PVDF 5130, Solvay) as binder. The slurries were mixed (0.5 h, 600 rpm) with the solvent N-Methyl-2-pyrrolidon (NMP 99.5%, VWR Chemicals) in a planetary ball mill (TMAX-DSP-LBPBM06A, Tmax Battery Equipments). The active material/conductive additive/binder ratio was 77/11.5/11.5 wt.-%. After mixing, the slurries were coated (6 cm $min^{-1}$, 500 µm) on an Al-foil (15 µm, MTI Corp.) with an automatic film coater (JK-TMJ-20, Tmax Battery Equipments). Finally, the electrode foils were dried under vacuum at 80° C for at least 24 h. Coin cells (CR2032, Hohsen) or Swagelok® cells were assembled in an argon-filled glovebox (< 1ppm $H_2O$, < 2 ppm $O_2$). A borosilicate-microfiber filter (CAT No. 5401-090 E, Whatman) was used as the separator. The electrolyte was 1M $LiPF_6$ conductive salt in a 1:1 wt% solution of ethylene carbonate and diethylene carbonate. In some cases, a sheet of metallic Lithium (99.9%, Aldrich) was used as the counter electrode (see below).

The electrodes were analyzed by scanning electron microscopy (NVision40, Zeiss). The cross-sectional preparation of the electrodes was performed using the broad ion preparation method (TIC020, Leica). Fig. S1. shows cross sectional images of the electrodes investigated. A homogeneous distribution of the active material particles (light grey) in the carbon-binder phase is observed.

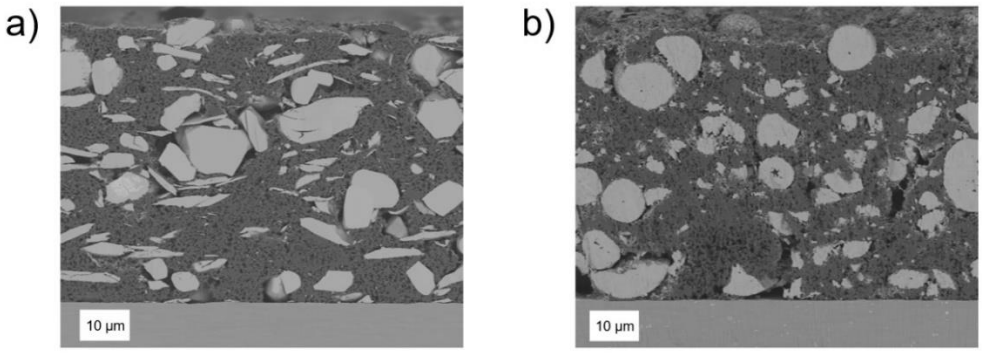


**Fig. S1.** Cross sectional SEM images of a) LCO and b) NCM electrodes.

Phase analysis was carried out using a D8 Advance diffractometer (Bruker) with a Cu-Kα X-ray tube and a 1D-detector. Fig. S2 shows XRD pattern obtained from electrodes investigated. The XRD patterns are consistent with theoretical patterns.

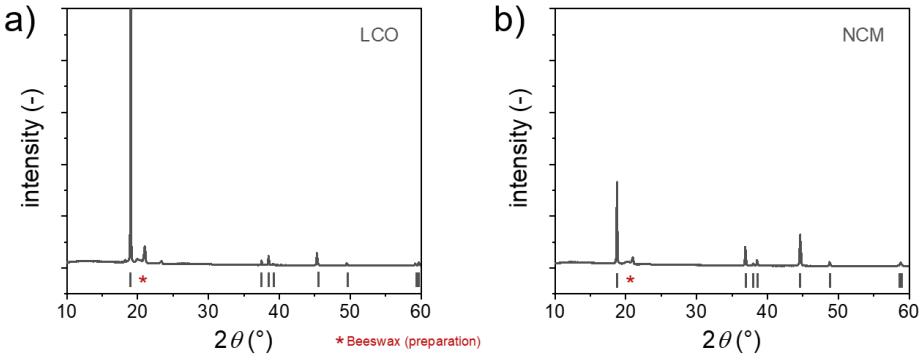


**Fig. S2.** Results of XRD analyses of as prepared electrodes made of a) $LiCoO_2$ (LCO) and b) $LiNi_{1/3}Co_{1/3}Mn_{1/3}O_2$ (NCM).

*Demonstration of working principle*

Two Swagelok® cells with LCO and NCM electrodes against Li-metal were assembled to adjust the chemical potential of Li in the materials. For this purpose, the cells were charged (Li extraction from the materials) until an electrode potential of 3.9 V was reached, which corresponds to the compositions $Li_{0.95}CoO_2$ and $Li_{0.63}Ni_{1/3}Co_{1/3}Mn_{1/3}O_2$, respectively. The electrochemical measurements were performed using a potentiostat with integrated frequency response analyzer (VMP3, Biologic). The change in stoichiometry was determined from the converted charge according to Faraday's law. After stoichiometry adjustment, the Swagelok® cells were disassembled to obtain the sub-stoichiometric electrodes. The sub-stoichiometric LCO and NCM electrodes were incorporated into coin cells as cathode (NCM) and anode (LCO) with fresh electrolyte and separator. The cells were then placed in a climate test chamber (CTC256, Memmert). Afterwards temperature cycling tests were carried out. First, the temperature was increased from 20 to 60 °C at $dT/dt$ = 0.5 K $min^{-1}$and the cell voltage was measured. The cells were then discharged at 60°C with -1 µA $cm^{-2}$ until a voltage of 0 V has been reached. Afterwards, the temperature was reduced to 20°C again and the cell was discharged until a voltage of 0 V has been reached again.

Based on the measurement data, the transferred electric charge, $\Delta Q$, is determined by integrating the electric current during constant temperature discharging according to:

$$\Delta Q = \int I \, \mathrm{d}t \tag{S1}$$

with *I* and *t* being the current and the time. The electric power is then given by:

$$P = IU \tag{S2}$$

with *U* being the cell voltage. The volumetric energy grained results to:

$$e = \frac{\Delta Q \bar{U}}{V} \tag{S3}$$

with *V* being the volume and $\bar{U}$ being the average cell voltage. The thermal-electrical conversion efficiency with respect to the Carnot limit can be defined as follows.

$$\varepsilon_{\mathrm{Carnot}} = \frac{e}{C\Delta \mathrm{T}\left(1-\frac{T_{\mathrm{low}}}{T_{\mathrm{high}}}\right)} \tag{S4}$$

with C being the volumetric heat capacity.

*Long term temperature cycling*

Long-term temperature cycling was performed by integrating an additional resistor (465 Ω) in parallel connection into the system as a model consumer (Fig. S3.).

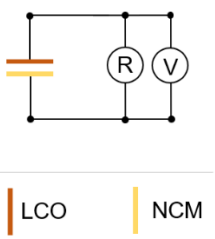


**Fig. S3.** Electrical equivalent circuit used for long term temperature cycling experiments. A resistor (465 Ω) is connected in parallel into the system as a model consumer.

The temperature regime for one cycle consists of 1 h 20 °C → 20 °C to 60 °C with d$T$/d$t$ = 0.5 K min$^{-1}$ → 1 h 60 °C → 60 °C to 20 °C with d$T$/d$t$ = 0.5 K min$^{-1}$. The energy gain has been determined by Equation S3. Fig. S4. shows the accumulated energy after 500 h long term temperature cycling.

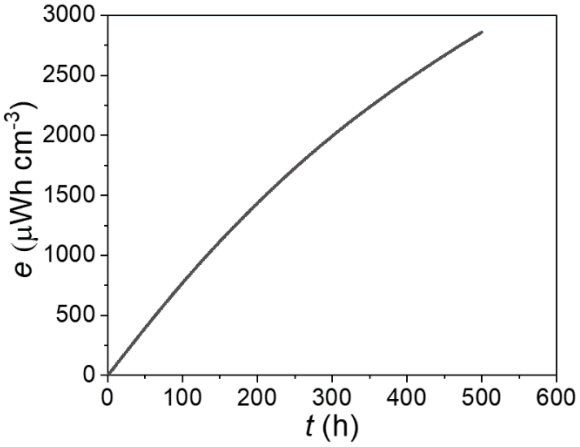


**Fig. S4.** Accumulated energy, *e,* during long-term temperature cycling in the electrical circuit shown in Fig. S3.

*Systematic studies on $\mu_{Li}$ dependence*

For the sake of simplicity, systematic studies on the dependence of the $\mu_{Li}$ dependence of $Li_xCoO_2$ | $Li_xNi_{1/3}Co_{1/3}Mn_{1/3}O_2$ cells were performed in a different experimental setup. NCM and LCO electrodes were assembled in coin cells against metallic Lithium. The cells were connected in an electrical equivalent circuit as shown in Fig. S5.

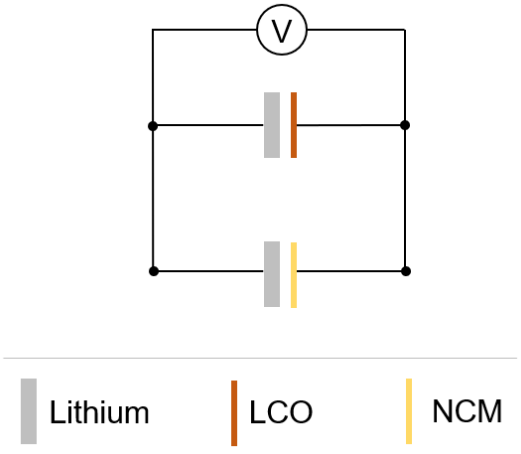


**Fig. S5.** Scheme for connection of electrochemical cells in parallel to set different electrochemical potentials of Li ($\mu_{Li}$) and corresponding x in $Li_xCoO_2$ and $Li_xNi_{1/3}Co_{1/3}Mn_{1/3}O_2$, respectively.

The parallel connection of the $Li_xCoO_2$ |Li and $Li_xNi_{1/3}Co_{1/3}Mn_{1/3}O_2$ | Li cells allows to set varying $\mu_{Li}$ dependence and corresponding x in $Li_xCoO_2$ and $Li_xNi_{1/3}Co_{1/3}Mn_{1/3}O_2$, respectively, by charging to defined electrode potentials (Li-extraction) while guaranteeing similar electrochemical potential of Li ($\mu_{Li}$) in both electrode materials. Fig. S6 shows the stoichiometry in the active materials LCO and NCM as a function of the chemical potential $\mu_{Li}$.

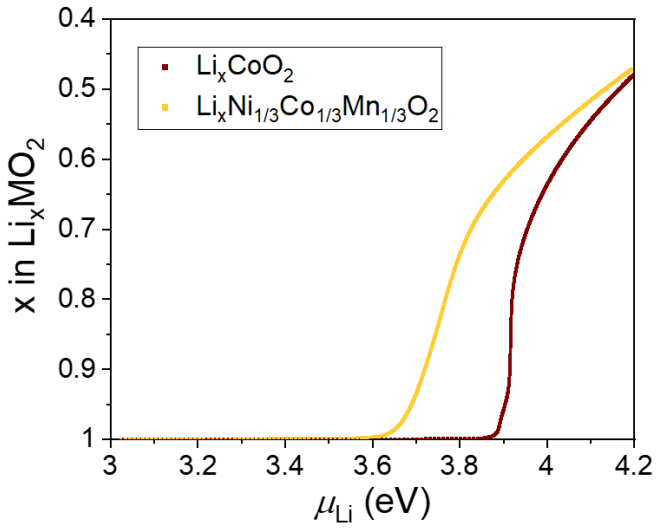


**Fig. S6.** Stoichiometry in the active materials LCO and NCM as a function of the chemical potential $\mu_{Li}$.

After adjustment of a certain electrochemical potential of Li ($\mu_{Li}$), the cell connection was switched to the electrical equivalent circuit shown in Fig. S7.

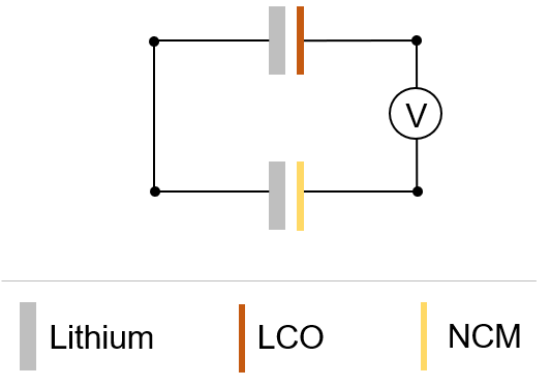


**Fig. S7.** Scheme for connection of electrochemical cells in series to investigate thermal-electrical energy conversion $Li_xCoO_2$ | $Li_xNi_{1/3}Co_{1/3}Mn_{1/3}O_2$ cells as a function of the electrochemical potential of Li ($\mu_{Li}$).

The series connection of $Li_xCoO_2$|Li and $Li_xNi_{1/3}Co_{1/3}Mn_{1/3}O_2$|Li cells shown in Fig. S7 allows investigations of the thermal-electrical energy conversion $Li_xCoO_2$ | $Li_xNi_{1/3}Co_{1/3}Mn_{1/3}O_2$ cells because the similar potentials of both Li electrodes cancel out each other in the circuit. Using this setup, temperature cycling tests were carried out similar to the tests described above. First, the temperature was increased from 20 to 60 °C at $dT/dt$ = 0.5 K $min^{-1}$and the cell voltage was measured. The cells were then discharged at 60°C with -1 µA $cm^{-2}$ until a voltage of 0 V has been reached. Afterwards, the temperature was reduced to 20°C again and the cell was discharged until a voltage of 0 V has been reached again. This process was repeated for different stoichiometries set by switching back to parallel connection as described above. In each case, based on the measured current and voltage, the power gain and volumetric energy accumulated was determined according to Equations S2 and S4 for the different electrochemical potential of the materials.

## Modeling

For the theoretical estimation of the thermal-electrical conversion effect based on intercalation chemistry, we make use of fundamental relationships based on equilibrium thermodynamics. The following mathematical derivation quantifies our model illustrated in Fig. 2a in the main paper.

The potential change, $\mathrm{d}E$, of an electrode with respect to a reference subjected to a temperature, $\mathrm{d}T$, change is given by:

$$\mathrm{d}E = \frac{\Delta_\mathrm{R}S}{zF}\mathrm{d}T \tag{S5}$$

with $\Delta_\mathrm{R}S$ being the entropy of reaction of the spontaneous half cell reaction and z and F being the valence (z = 1 in the case of $Li^+$) and the Faraday constant (96.485 As $mol^{-1}$).

The cell voltage between electrodes A and B is given by:

$$U = E_\mathrm{A} - E_\mathrm{B} \tag{S6}$$

Neglecting the temperature dependence of the reaction entropy, the change in cell voltage, $\Delta U$, resulting from the temperature change, $\Delta T$, is given implementing Eq. S5 into S6:

$$\Delta U = \frac{1}{zF}(\Delta_\mathrm{R}S_\mathrm{A} - \Delta_\mathrm{R}S_\mathrm{B})\Delta T = \Delta E_\mathrm{A} - \Delta E_\mathrm{B} \tag{S7}$$

According to equation S7, any difference in the reaction entropies of electrodes A and B leads to the buildup of a cell voltage. In the case of Li-intercalation electrodes this cell voltages can be reduced by closing the external circuit, allowing the exchange of electrons between the electrode materials A and B and corresponding redox reactions. The electric charge converted by the electrode materials associated with this process is given by:

$$\Delta Q_\mathrm{A} = \left(\frac{\mathrm{d}Q_\mathrm{A}}{\mathrm{d}E_\mathrm{A}}\right)\Delta E_\mathrm{A} \tag{S8.1}$$

$$\Delta Q_\mathrm{B} = \left(\frac{\mathrm{d}Q_\mathrm{B}}{\mathrm{d}E_\mathrm{B}}\right)\Delta E_\mathrm{B} \tag{S8.2}$$

with $\mathrm{d}Q_\mathrm{A}/\mathrm{d}E_\mathrm{A}$ and $\mathrm{d}Q_\mathrm{B}/\mathrm{d}E_\mathrm{B}$ being the differential capacities of the materials A and B, respectively. The electric charge consumed by material A must be provided by material B. Therefore, the principle of conservation of charge states that the exchanged electric charge between the electrodes, $\Delta Q$, is given by:

$$\Delta Q = \left(\frac{\mathrm{d}Q_\mathrm{A}}{\mathrm{d}E_\mathrm{A}}\right)\Delta E_\mathrm{A} = -\left(\frac{\mathrm{d}Q_\mathrm{B}}{\mathrm{d}E_\mathrm{B}}\right)\Delta E_\mathrm{B} \tag{S9}$$

Replacing $\Delta E_\mathrm{B}$ in Eq. S9 by Eq. S7 results in:

$$\Delta Q = \frac{1}{zF}(\Delta_\mathrm{R}S_\mathrm{A} - \Delta_\mathrm{R}S_\mathrm{B})\Delta T\,\frac{\left(\frac{\mathrm{d}Q_\mathrm{A}}{\mathrm{d}E_\mathrm{A}}\right)\left(\frac{\mathrm{d}Q_\mathrm{B}}{\mathrm{d}E_\mathrm{B}}\right)}{\left(\frac{\mathrm{d}Q_\mathrm{B}}{\mathrm{d}E_\mathrm{B}}+\frac{\mathrm{d}Q_\mathrm{A}}{\mathrm{d}E_\mathrm{A}}\right)} \tag{S10}$$

Based on Eq. S10 and assuming a linear decrease in voltage during discharge, the effective average voltage during the discharge process, $\overline{U}$, is the equal to:

$$\overline{U} = \frac{1}{2zF}(\Delta_\mathrm{R}S_\mathrm{A} - \Delta_\mathrm{R}S_\mathrm{B})\Delta T \tag{S11}$$

The energy obtained from the cell during discharging to 0 V after a temperature change ($\Delta T$) with respect to the volume, *V*, is then given by:

$$e = \Delta Q\overline{U} = \frac{1}{2z^2F^2V}(\Delta_R S_A - \Delta_R S_B)^2 \Delta T^2 \frac{\left(\frac{dQ_A}{dE_A}\right)\left(\frac{dQ_B}{dE_B}\right)}{\left(\frac{dQ_B}{dE_B}+\frac{dQ_A}{dE_A}\right)} \quad \text{(S12)}$$

The thermal-electrical conversion efficiency with respect to the Carnot limit can be defined as follows.

$$\varepsilon_{Carnot} = \frac{e}{C\Delta T\left(1-\frac{T_{low}}{T_{high}}\right)} \quad \text{(S13)}$$

with C being the volumetric heat capacity.

The above equations were used to compute or predict the cell voltage, electric charge consumed and energy obtained during discharging after a temperature change as well as estimating the thermal-electrical conversion efficiency with respect to the Carnot limit. The Equation S12 states the energy obtained from discharging the cell to 0 V after a temperature change ($\Delta T$) in terms of volume specific values (e.g. µWh $cm^{-3}$). Equation S13 states the thermal-electrical conversion efficiency with considering a certain heat capacity. Obviously, the choice of volume has a significant influence on the resulting volumetric energy density and conversion efficiency. Relating the quantities to the volume of the active materials in the anode and cathode is representative of the material combination and represents an optimum of the performance. This consideration is target-oriented for fundamental studies, as presented in the main paper. For practical applications, reference to the complete cell volume is purposeful, and the contribution of the construction and the inactive materials must be considered. In the present fundamental study, demonstrating thermal-electrical energy conversion based on intercalation chemistry, the achieved energy density and conversion efficiency were reported with reference to the volume of the active materials in the anode and cathode. Considering the inactive materials, the achieved energy density and conversion efficiency, due to the non-optimized electrode and cell design, are significantly reduced (cf. Fig. S8 and Tab. S1). In our laboratory level study, model electrodes (low electrode thickness, high porosity, excess of binder and conductive additives) and cell a design with excess electrolyte (thick and high porosity separator) were used. This leads to a drastic reduction of the achieved energy density and the conversion efficiency when referring to the complete cell volume. Optimized electrode and cell designs can significantly improve the ratio of active to inactive materials, which consequently leads to a much higher practical energy density and conversion efficiency at the cell level. Figure S8 illustrates these relationships using the material level as an example compared to the cell level for the design used in this study and an optimized design. Table 1 shows the respective design parameters of the different scenarios. By optimizing the electrode and cell design, the practical energy density and conversion efficiency at the cell level can be significantly improved compared to the model systems studied here.

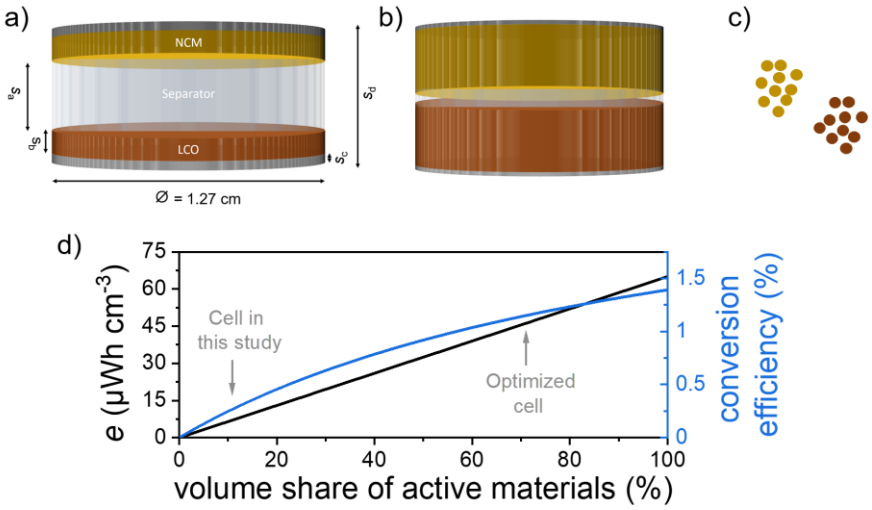


**Fig. S8.** Schematic illustrations of a) electrochemical cell design and geometrical dimensions ($s_a$ = thickness of separator, $s_b$ = thickness of electrode layer, $s_c$ = thickness of current collector, $s_d$ = total cell thickness) used in this study b) optimized cell design based on ongoing work in the field of lithium-ion battery technology c) raw materials. d) Volumetric energy and conversion efficiency with respect to the Carnot limit as a function of the volume share of active materials in the cell.

**Tab. S1.** Geometrical dimensions of cell components ($s_a$=thickness separator, $s_b$=thickness electrode layer, $s_c$=thickness current collector, $s_d$=total cell thickness) for various cell designs, with volume shares of active material, binder, and conductive additive in the electrode layer as well as volume share of active material in relation to the total cell volume.

| | $s_a$ (µm) | $s_b$ (µm) | $s_c$ (µm) | $s_d$ (µm) | *Electrode porosity* (%) | $V_{share}$ active material / electrode (%) | $V_{share}$ binder/ electrode (%) | $V_{share}$ conductive additive/ electrode (%) | **$V_{share}$ active material/ $V_{total}$ (%)** |
|---|---|---|---|---|---|---|---|---|---|
| Materials level | - | - | - | - | - | - | - | - | **100** |
| Cell-design in this study | 150 | 50 | 10 | 270 | 60 | 23.3 | 8.8 | 7.8 | **10.4** |
| Optimized cell-design | 10 | 200 | 5 | 420 | 15 | 81 | 2.1 | 1.9 | **72.1** |

*Determination of electrochemical material parameters*

Appropriate input parameters were required to calculate the theoretical values for the voltage buildups, transferred electric charge, and energy density resulting from the above model descriptions. For this purpose, NCM and LCO electrodes were assembled in coin cells against metallic Lithium. These cells were used to determine the required parameters using electrochemical methods. For the determination of the reaction entropy, the electrodes were delithiated galvanostatically (15 mA $g^{-1}$) to different cell potentials, followed by a 12 h relaxation period to achieve electrochemical equilibrium. Subsequently, a temperature-dependent measurement of the cell potential has been performed. The temperature was varied linearly between 15 and 35 °C with $dT/dt$ = 0.5 K $min^{-1}$, while recording the cell potential. Figure S9 shows an exemplary measurement of the temperature dependence of the cell

potential. Based on these data, the reaction entropy for different preset $\mu_{Li}$ and x in $Li_xCoO_2$ and $Li_xNi_{1/3}Co_{1/3}Mn_{1/3}O_2$, respectively, was determined using the following relationship:

$$\Delta S = zF \frac{\mathrm{d}E}{\mathrm{d}T} \tag{S14}$$

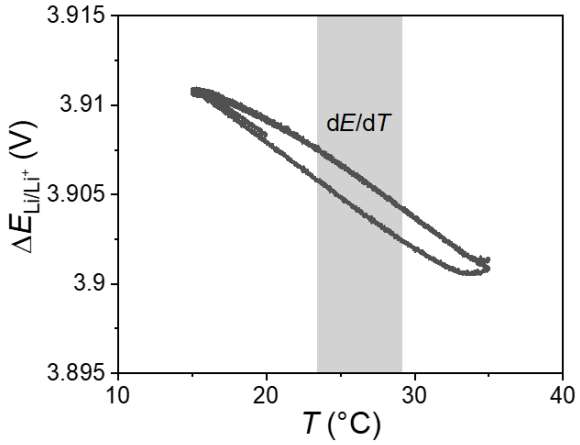


**Fig. S9.** Electrode potential plotted against the imposed temperature for $Li_{0.95}CoO_2$ ($\mu_{Li}$ = 3.9 eV), the region used for the determination of d$E$/d$T$ is highlighted in grey.

For the determination of the differential capacity, the electrodes were delithiated stepwise (15 mA $g^{-1}$ for 30 times) each time followed by a relaxation period (12 h) to achieve electrochemical equilibrium. The differential capacity was determined from the change in open circuit potential with respect to the specific charge consumed according to:

$$Q = \int \left(\frac{\mathrm{d}Q}{\mathrm{d}E}\right) \mathrm{d}E \tag{S15}$$

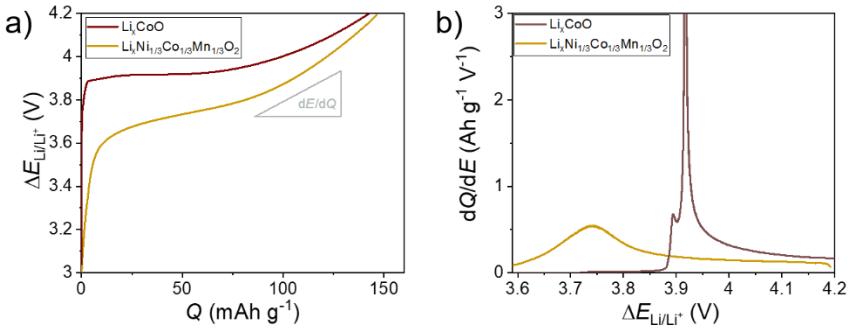


**Fig. S10.** Determination of the differential capacity with a) electrode potential of LCO and NCM plotted against the specific capacity and b) differential capacity of LCO and NCM plotted against the electrode potential.